Electric Spark Deposition of Antibacterial Silver Coating on Microstructured Titanium Surfaces with a Novel Flexible Brush Electrode

Kaihui Shi,[§] Hao Zhang,[§] Yuyan Gu, Zhijie Liang, Huanyu Zhou, Haojie Liu, Jiangwen Liu, and Guie Xie*

Read Online

ACCESS | Metrics & More | Article Recommendations

ABSTRACT: Infection caused by orthopedic titanium implants, which results in tissue damage, is a key factor in endosseous implant failure. Given the seriousness of implant infections and the limitations of antibiotic therapy, surface microstructures and antimicrobial silver coatings have emerged as prominent research areas and have displayed certain antimicrobial effects. Researchers are now working to combine the two to produce more effective antimicrobial surfaces. However, building robust and homogeneous coatings on complex microstructured surfaces is a tough task due to the limits of surface modification techniques. In this study, a novel flexible electrode brush (silver brush) instead of a traditional hard electrode was designed with electrical discharge machining, which has the ability to adapt to complex groove interiors. The results showed that the use of flexible electrode brush allowed silver to be deposited uniformly in titanium alloy microgrooves. On the surface of Ag-TC4, a uniformly covered deposit was visible, and it slowly released silver ions into a liquid environment. In vitro bacterial assays showed that a Ag-TC4 microstructured surface reduced bacterial adhesion and bacterial biofilm formation, and the antibacterial activity of Ag-TC4 against *Staphylococcus aureus* and *Escherichia coli* was 99.68% $\pm$ 0.002 and 99.50% $\pm$ 0.007, respectively. This research could lay the groundwork for the study of antimicrobial metal bound to microstructured surfaces and pave the way for future implant surface design.
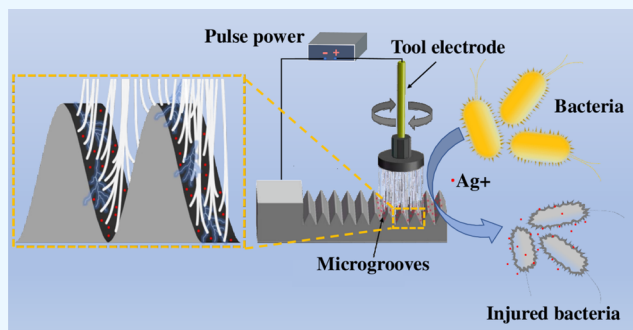
1. INTRODUCTION

Bone illnesses and bone defects are seriously affecting people's health, and the number of bone implant cases has increased greatly in recent years. Therefore, the research on biomedical materials is extremely urgent.[1] Biomedical materials are widely used in orthopedics, plastic surgery, dentistry, cardiovascular stents, medical devices, and so forth. They mainly include natural derivatives,[2] polymer organic materials,[3] inorganic materials and their composites,[4] as well as metals. Among them, metallic materials, especially titanium and its alloys, are widely used in medical implants because of their low density, good strength, high toughness, good corrosion resistance, and low modulus of elasticity.[5]

However, titanium lacks antimicrobial properties, therefore, bacteria are more likely to colonize the material surface. Following colonization, the bacteria can grow to form a biofilm that leads to subsequent implant infections and peritissue inflammation.[6,7] In fact, implant infections are one of the most common and serious complications associated with the use of biomaterials, accounting for 25.6% of all health care-associated infections and often leading to implant failure, secondary surgery, and serious or life-threatening patient health

problems.[7] Antibiotic medication is the conventional clinical treatment for implant infections, but it is poorly targeted, potentially hepatotoxic and nephrotoxic, and more importantly, difficult to treat due to bacterial resistance, tolerance, and persistence, as well as biofilm formation.[8,9]

Given the seriousness of implant infections and the limitations of antibiotic therapy, there is an urgent need to explore new strategies to prevent implant infections in addition to the use of antibiotics. In recent years, the use of surface micro- and nanomorphology or surface chemistry for the improvement of the antimicrobial properties of implants has attracted increasing interest.[10,11] Some researchers have worked on biomimetic micro- and nanostructures inspired by natural antifouling surfaces,[12] such as cicada wings,[13] dragonfly
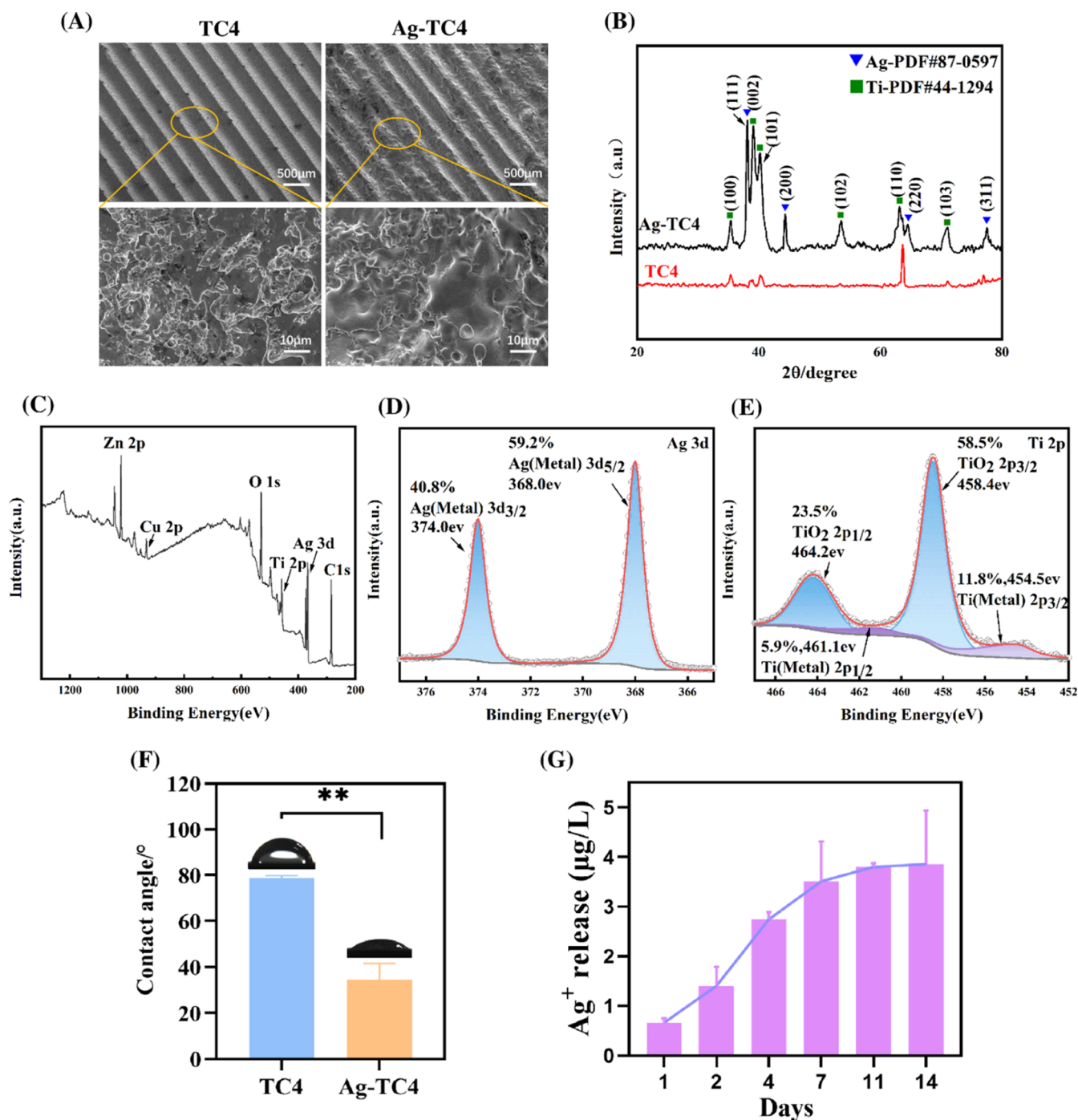
Figure 1. Morphological and microstructural characterization of TC4 and Ag-TC4: (A) surface views and (B) XRD pattern of Ag-TC4 surface with silver wire. XPS results: (C) full spectrum, (D) Ag 3d spectrum, and (E) Ti 2p spectrum. (F) Contact angle of TC4 and Ag-TC4 samples. (G) Accumulation of released silver ions from Ag-TC4 samples immersed in deionized water. (Values are mean ± standard deviation, **represents $P <$ 0.01, TC4 vs Ag-TC4, every result was obtained from three independent experiments).

wings,[14] and gecko skin structures.[15] The effect of material surfaces on bacterial colonization appears to depend on the size of surface structures, surface roughness, hydrophilicity, hydrophobicity, and chemical composition of material surfaces, as well as the interaction of bacteria with material surfaces. Ge[16] et al. studied submicron-sized arrays of silica periodic columns and found that they could inhibit bacterial adhesion and proliferation through spatially restricted size effects. Jannesari[17] et al. applied rGO/CuO$_2$ nanocomposite as an oxygen nanoshuttle applicable in controllable transfer of

O$_2$NBs to battle against drug-resistant bacterial infections, the combination of CuO$_2$ (as a solid source of oxygen) and rGO nanosheets effectively controlled and prolonged in situ oxygen release, which provides a long-lasting antibacterial effect. Akhavan and Ghaderi[18] investigated the interaction between chemically exfoliated graphene oxide (GO) nanosheets and *Escherichia coli* living mixed-acid fermentation with an anaerobic condition at different exposure times and showed that GO sheets could act as biocompatible sites for adsorption and proliferation of the bacteria on their surface, while

bacterially reduced GO sheets inhibited bacterial proliferation on their surface.

Moreover, microstructures also play an important role in inducing directional cell alignment and differentiation.[19] Jayaraman[20] et al. found that surfaces with microgrooves promoted osteoblast adhesion, proliferation, and mineralization of bone tissue better than the rough surface treated with sandblasting and acid etching. Similarly, Li[21] et al. found that concentric microgrooved surface of polycaprolactone promoted osteogenic differentiation of mMSCs, including upregulation of early osteogenic marker genes by combining photolithography with a fusion casting method to simulate the concentric microgrooved structure of bones in a two-dimensional environment.

In addition to the construction of micro/nanostructures, materials can also be given antimicrobial properties by coating or adding metals or alloys. Silver is known to be an effective antimicrobial agent and plays an important role in improving the antimicrobial properties of implants, effectively inhibiting the growth of Gram-positive and -negative bacteria and the formation of their biofilm.[22] It has been shown that silver can bind to multiple sites in bacterial cells at very low concentration levels and inhibit bacterial growth.[23] Kang[24] et al. found that the acid-etched Ti–Ag alloy had a better antibacterial effect due to the release of high concentrations of silver ions. Akhavan[25] reported the Ag–TiO$_2$/Ag/a-TiO$_2$ nanocomposite thin film photocatalyst sensitive to the solar light with an efficient storage of Ag nanoparticles both on the film surface and at interface of the Ag–TiO$_2$, and a-TiO$_2$ thin films was simply synthesized by sol–gel, the nanocomposite facilitated the release of more silver ions and thus exhibited a better antibacterial action.

Given that both surface microstructures and silver have certain antibacterial properties, researchers have worked to combine the two to produce more durable and stable antibacterial surfaces. Jin[26] et al. used GO thin film and silver (Ag) nanoparticles to modify the Ti substrate surface by electroplating and UV reduction methods. The results show that the antimicrobial activity and relative adhesion rate of GO–Ag–Ti are very prominent against *Streptococcus mutans* and *Porphyromonas gingivalis*. Electroplating can make antibacterial metal coating uniformly combined in the microstructure surface, but titanium surface is often covered with a dense, strong adhesion, tough thin oxide film (TiO$_2$), so it is difficult to plate metal on the surface of titanium alloy, and even if it can be coated, the coating bond is often very poor. Researchers have made many attempts to overcome this challenge. Akhavan[27] deposited a mesoporous TiO$_2$ cap layer on the grown Ag nanorods in order to protect the silver coating and achieve effective control of silver ion release. Similar to this, Park[28] et al. fabricated mesoporous thin films composed of TiO$_2$ nanoparticles on the anodized titanium implant surface for loading silver nanoparticles to achieve long-lasting antibacterial efficacy. In addition, electrical discharge machining (EDM) is also a promising method because the EDM deposited layer is metallurgically bonded to the substrate with high bond strength and does not flake easily. However, traditional EDM often uses a hard electrode, and it has some problems such as an uncontrollable discharge gap, an unstable deposition transition process, and unevenly deposited material, making its application in complex surface processing limited.[29] Therefore, in order to solve the abovementioned problems and to compensate for the defects of electroplating and

conventional EDM, we design a flexible brush electrode (silver brush), which has the ability to adapt to complex groove interiors in EDM. The use of the flexible brush electrode in EDM allows the antimicrobial silver to be deposited uniformly onto the titanium microgrooved surface in a metallurgical bond that is strong and resistant to peeling.

In this study, Gram-positive *Staphylococcus aureus* (*S. aureus*) and Gram-negative *Escherichia coli*, the most common pathogens in implant-associated infections, were selected as models to investigate the effects of a silver-coated microgrooved surface on bacterial adhesion, growth, and morphology, as well as on bacterial biofilm formation and related gene expression, providing a deeper theoretical basis for the application of the modified microgrooves.

2. RESULTS AND DISCUSSION

2.1. Characterization of Samples. A sinusoidal microgrooved structure with a width (w) of 200 μm and a depth (h) of 400 μm was obtained on the titanium alloy after wire EDM (WEDM), where L (=10 mm) is the width of the samples (Figure 7B,C). After EDM deposition, a uniform layer of silver-white deposit was visible on the surface of the microgrooves. The deposit was a thin layer retaining the original morphology of the microgrooves, as shown in Figure 1A. Under high magnification, the rough deposits were of different sizes, with some of the silver remelting and aggregating into larger silver deposits during multiple discharge processes.

Figure 1B shows the diffraction peak curve of the Ag-TC4 surface, compared with the standard curve of the silver wire, and it was found that the two coincided at the silver diffraction peak, indicating that the silver-white deposits on the surface of the microgrooves contained silver. Thus far, we have successfully constructed a silver-containing microgrooved surface on titanium alloy substrates using the EDM technique.

Figure 1C depicts the results of the full spectrum scan analysis of the surface of Ag-TC4 samples. The results show that the samples' surfaces comprise zinc (Zn), copper (Cu), oxygen (O), titanium (Ti), silver (Ag), and carbon (C). Of these, zinc and copper were introduced through the use of a wire EDM system in the preparation of sinusoidal microgrooves, because the brass electrode wire utilized in the production of the sinusoidal microgrooved surface consists of copper and zinc. When the sample was exposed to air after processing, it oxidized, allowing carbon and oxygen to be detected. Figure 1D depicts the fine spectrum of Ag 3d. The absorption energies of the Ag 3d$_{3/2}$ and Ag 3d$_{5/2}$ orbitals are 374 and 368 eV, respectively, which are compatible with the absorption peak of the silver monomer. The results show that after EDM deposition, the silver on the surface of the samples is mainly in the form of monomers. Figure 1E shows the fine spectrum of Ti 2p, which reveals that the titanium on the surface of the samples is mainly in the form of TiO$_2$ and a small amount of metallic titanium.

The contact angles of TC4 and Ag-TC4 samples were measured using a contact angle meter, and the results were 78.67 $\pm$ 1.08° and 34.45 $\pm$ 7.14°, respectively (Figure 1F), indicating better wetting properties on the surface of the samples after EDM silver deposition.

Much research has demonstrated that silver ions or silver nanoparticles may destroy bacteria.[30] It is generally accepted that the antibacterial effect of Ag-containing coatings or alloys is primarily due to the release of silver ions and that the
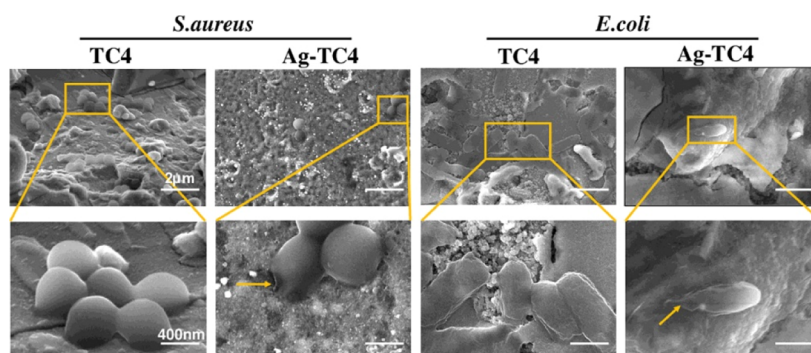
Figure 2. SEM micrographs of *S. aureus* and *E. coli* on the surface of TC4 and Ag-TC4 samples.
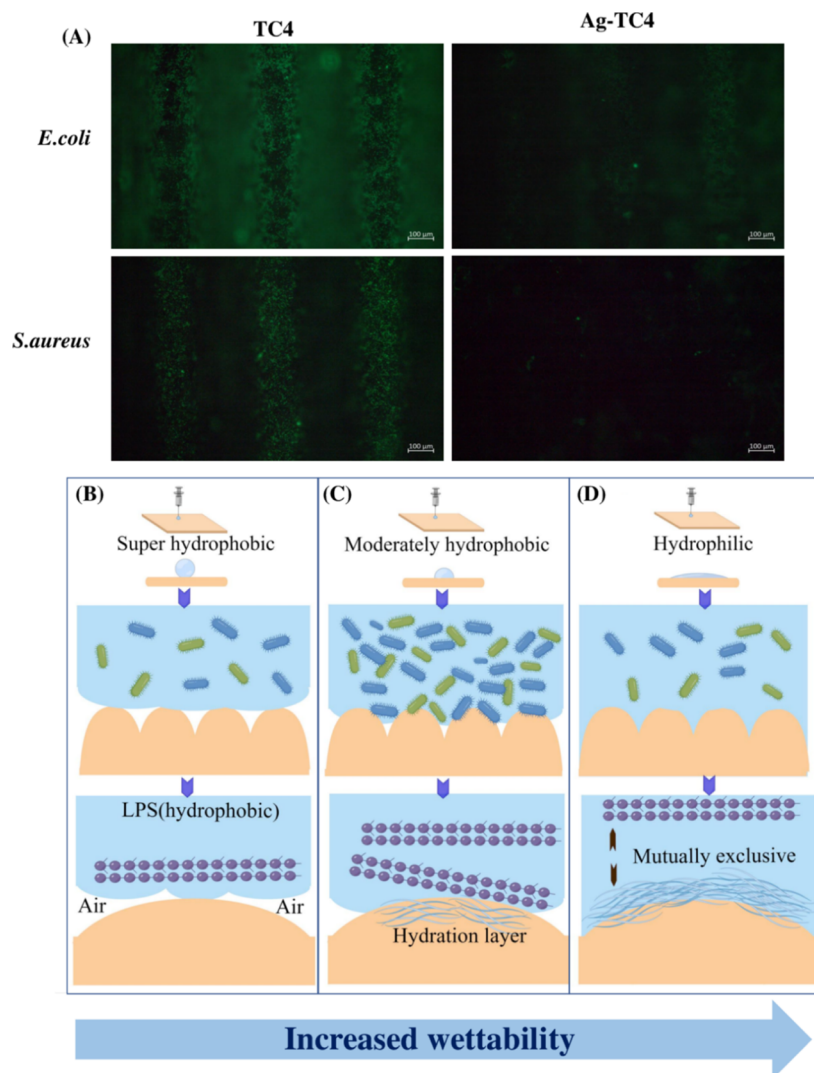

Figure 3. Early bacterial adhesion: (A) SYTO9 fluorescent staining of *E. coli* and *S. aureus* adhering to TC4 and Ag-TC4 samples. (B) Schematic illustration of the effect of a superhydrophobic surface on bacterial adhesion. (C) Schematic illustration of the effect of a moderately hydrophobic surface on bacterial adhesion. (D) Schematic illustration of the effect of a hydrophilic surface on bacterial adhesion. (B−D were made by Figdraw). Experiments were repeated three times, and each sample was observed in five random fields under the fluorescence microscope.

amount of silver ions released is directly connected to the bactericidal capabilities.[31,32] After EDM silver deposition, the surface of the microgrooves was covered with metallic silver, which was hydrolyzed to produce and release silver ions when coming into contact with the aqueous environment. In this study, the release of silver ions from the microgrooved surface

for different immersion time in deionized water is shown in Figure 1G. The release of silver ions appears to be time-dependent. A sharp increase in silver ion concentration was observed within the first four days, and then, its release slowed down, and a plateau was reached in 2 weeks with a cumulative concentration of 3.85 μg/L, a concentration level that is

capable of rendering an antimicrobial efficacy and is below cytotoxic levels (3564 μg/L).[33] There are many studies showing that silver ions release can be related to many factors, such as the responsive release of pH and GSH.[34] Similar to Kumar's study,[35] in this work, metallic silver was oxidized in the aqueous medium to produce silver ions, so it was speculated that the release of silver ions may be related to the diffusion of the aqueous medium over the microgrooved surface. Although the diffusion of silver ions in this way can achieve a good antibacterial effect, there are still some inherent limitations, such as nontargeted silver ion release and biotoxicity due to accumulation. In fact, for both traditional AgNPs and Ag-loaded materials, the release of silver ions is difficult to control on demand.[36] Therefore, the study of the efficient and controlled release of silver ions is a promising direction.

2.2. Observation of Bacterial Morphology. Scanning electron microscopy (SEM) was used to observe the morphologies and membrane integrity of *S. aureus* and *E. coli* on the samples. The amount of *S. aureus* and *E. coli* adhering to the TC4 microgrooved surface was obviously more than that on the Ag-TC4 microgrooved surface. On the TC4 microgrooved surface, a large number of bacteria were attached, whose morphology was rounded, and the bacterial membranes were glossy and intact without obvious rupture. In contrast, on Ag-TC4 samples, the number of bacteria was significantly reduced, and the bacterial distribution was sparse. Meanwhile, the bacteria cells became irregular and distorted due to the disruption and lysis of bacterial membranes (Figure 2). These results suggest that silver deposited on the surface, to some extent, possessed the ability of impeding bacteria adhesion and lysing cell membranes, additionally potential for improving the antibacterial activities of Ti-based materials.

The effect of Ag-TC4 on bacterial morphology and membranes may be related to the interaction between Ag$^+$ and the cell walls. In the current study, the silver monomer deposited by EDM continuously released Ag$^+$ even after being immersed for 14 days in deionized water. Most bacteria suffered damage to cell walls and cell membranes or even lysis due to the toxic effects of Ag$^+$, as shown in Figure 2. This could be a result of the released Ag$^+$ interacting with cell walls and binding to β-1/4 bonds of *N*-ace-tylglucosamine and *N*-acetylMA of glycan strands, changing the conformation of the polypeptide portion of bacterial cell walls and glycan strands and thus causing damage to bacterial cell walls. Finally not only the secondary structure of bacterial cell walls (α-helical structure) but also the primary structure of cell walls was changed.[37] In addition, it has been demonstrated that bacteria produce more reactive oxygen species (ROS) when they come into contact with Ti—Ag samples that include a silver-rich phase. In bacterial cells, ROS enhances oxidative stress, which can disrupt the integrity of the cell membranes, leading to protein leakage, and eventually result in bacterial death.[32]

However, titanium lacks antimicrobial properties, therefore, bacteria are more likely to colonize the material's surface. Following colonization, the bacteria can grow to form a biofilm that leads to subsequent implant infections and peritissue inflammation.

2.3. Early Bacterial Adhesion. Bacterial adhesion to the surface of implant materials is the first step in the development of infection. During the implant treatment, bacteria from intraoperative or host bloodstream dispersal can easily colonize the implant surface. Following colonization, the bacteria can grow to form a three-dimensional structure of bacterial biofilm, which can then be dispersed by bacteria to proliferate at a distant location, and the cycle repeats itself; finally, an ecosystem of bacterial biofilm forms, leading to treatment failure and becoming a difficult clinical problem. Therefore, it is crucial to inhibit early bacterial adhesion to prevent implant infection and inflammation.

To further investigate the early bacterial adhesion on various surfaces, *S. aureus* and *E. coli* were stained with SYTO9. Bacterial densities on each sample are shown in Figure 3A. A large number of bacteria adhered to the TC4 samples, and the amount of adhered bacteria decreased significantly after EDM silver deposition on the microgrooves. This is consistent with the results of the abovementioned observations of bacterial morphology. The adherence of bacteria to material surfaces is usually considered to involve physical or chemical factors, such as surface morphology,[38] hydrophobic interaction, van der Waals forces, electrostatic interactions,[39] roughness, wettability,[40] and antiadhesive chemical composition.[41] After the EDM process, the microgrooved surface was coated with a layer of silver monomer that increased the roughness of the microgrooved surface, and the surface contact angle of the samples decreased from 78.67 $\pm$ 1.08° to 34.45 $\pm$ 7.14° after EDM silver deposition. Due to the great change in the wettability of the samples' surface, the hydrophilicity of the samples increased. Because of their self-cleaning ability, superhydrophobic surfaces are frequently believed to resist bacterial adhesion, whereas moderately hydrophobic surfaces (contact angles close to 90°) exhibit the highest levels of bacterial adhesion (Figure 3B,C). By studying how hydrophobic surfaces affected lipopolysaccharide (LPS), a crucial component of Gram-negative bacterial cell walls, Jiang[42] et al. discovered Gram-negative bacteria like *E. coli* were less likely to adhere because of the strong mutual repulsion between the hydrophobic LPS and the tightly hydrated layer formed by the hydrophilic surface (Figure 3D). Conversely, as the hydrophilicity decreased, the amount of LPS adsorbed on the surface increased, encouraging bacterial adhesion. Similar to this, the hydrated layer inhibits bacterial adhesion for Gram-positive bacteria, such as *S. aureus*, whose cell walls are primarily composed of peptidoglycan. As the hydrophilicity of the surface increases, the hydrogen bonding force between the peptidoglycan and the surface decreases, thus reducing bacterial adhesion.[43] In accordance with the abovementioned findings, we speculate that an increase in the samples' surface hydrophilicity within a certain range might enhance their resistance to bacterial adhesion.

2.4. Antimicrobial Activity. Although changing the physical properties of a material surface might somewhat lessen bacterial adherence, certain adherent bacteria can still multiply and spread rapidly to form a biofilm, which, once formed, severely limits the effect of antibiotics and makes infection treatment more challenging. As a result, it is essential to establish a second line of defense to kill the adherent bacteria and prevent infection from occurring. In current research on endosomal antimicrobial agents, the main antimicrobial substances are various antibiotics, such as gentamicin and ciprofloxacin, organic antimicrobial agents, and metal ionic antimicrobial agents, such as silver, copper, and zinc.[44] As the most widely used antimicrobial agent, silver has the advantages of a long-lasting and stable antimicrobial effect, broad-spectrum antimicrobial activity against Gram-negative and -positive bacteria, as well as some drug-resistant bacteria,
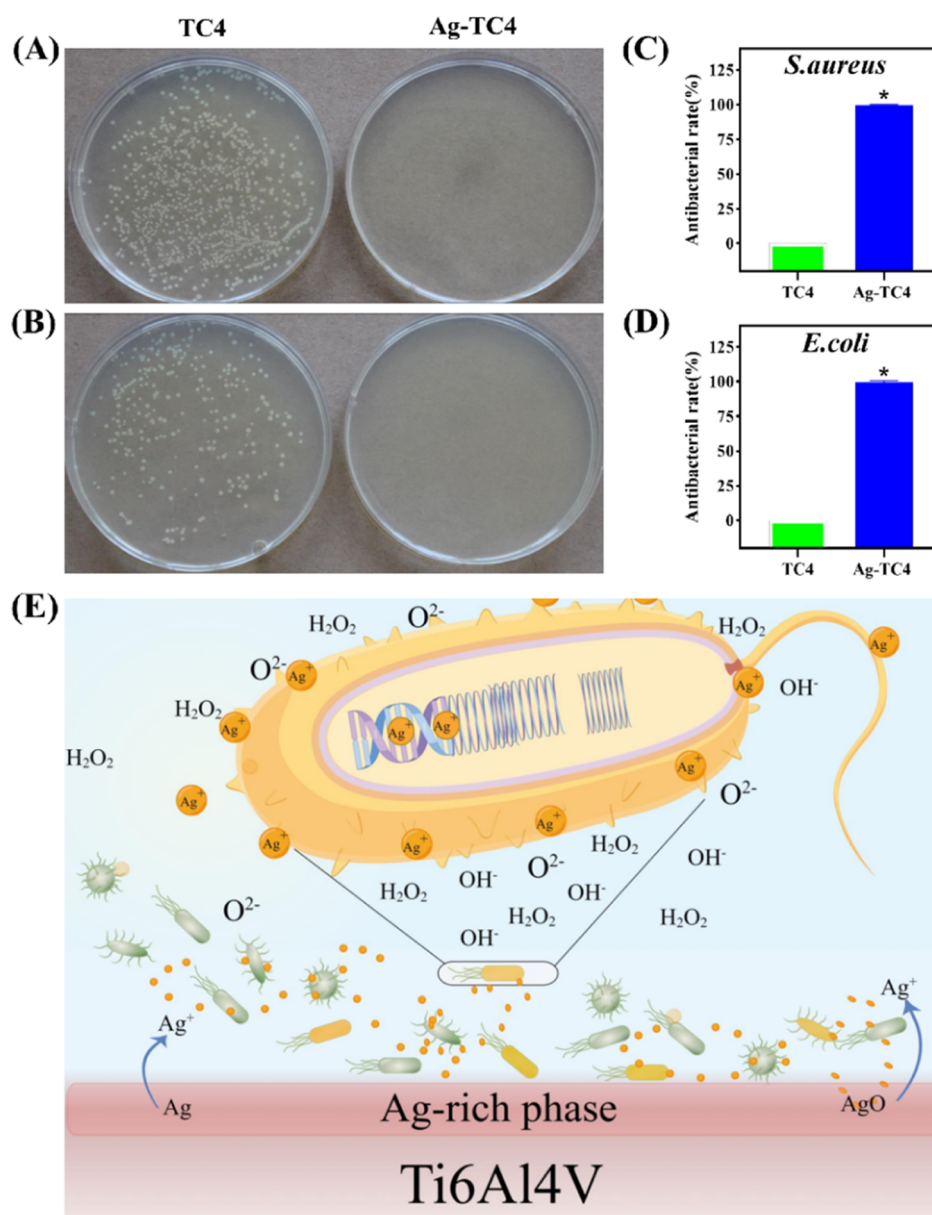
Figure 4. Antibacterial properties of TC4 and Ag-TC4 samples: (A,B) *S. aureus* and *E. coli* colonies on LB agar plates. (C,D) Antibacterial rate of *S. aureus* and *E. coli*. (Values are mean ± standard deviation, *represents *P* < 0.05, TC4 vs Ag-TC4, and every result was obtained from three independent experiments). (E) Schematic illustration of the principle of the antibacterial effect of Ag-TC4 (this diagram was made by Figdraw).

low drug resistance, and good heat resistance, which makes it a great candidate for endosomal antimicrobial applications.[45] In this study, silver was electrodeposited onto the titanium microgrooves, and plate counting was used to assess the modified microgrooves' antibacterial efficacy. Figure 4A,B show the bacterial colonies on TC4 and Ag-TC4 samples after 24 h incubation on LB agar plates. In contrast to the TC4 samples, which had a lot of bacterial growth, the Ag-TC4 samples showed very few or no growing colonies. The antibacterial activity of Ag-TC4 against *S. aureus* and *E. coli* was 99.68% ± 0.002 and 99.50% ± 0.007, respectively (Figure 4C,D).

It has been demonstrated that Ag^+ has bacteriolytic and damaging effects on bacterial cell walls in *S. aureus* and *E. coli* and can cause the production of ROS such as O^{2-}, H_2O_2, ^+OH, and OH^- in bacterial cell walls (Figure 4E). Additionally, Ag^+ has been shown to form Ag^+ coordination complexes in

the double and triple hydrogen bonds of DNA base pairs, which harm bacterial DNA.[46] In the current study, the extraordinarily potent antibacterial properties of the Ag-TC4 samples may be related to the damage that released Ag^+ did to bacterial cell walls.

2.5. Biofilm Live/Dead Staining. In infections associated with the medical implant, biofilm-related infections are highly resistant to host defenses and can inhibit host adaptive and innate immune responses, often leading to severe inflammatory responses that cause tissue damage and ultimately implant failure.[7] In addition, biofilms are highly resistant to antibiotic treatment[47] and recalcitrant to harsh environments, such as ultraviolet (UV) radiation, extreme temperature, extreme pH, high salinity, high pressure, and poor nutrients.[48] Prevention of bacterial biofilm formation is therefore one of the most active areas of implant material research.
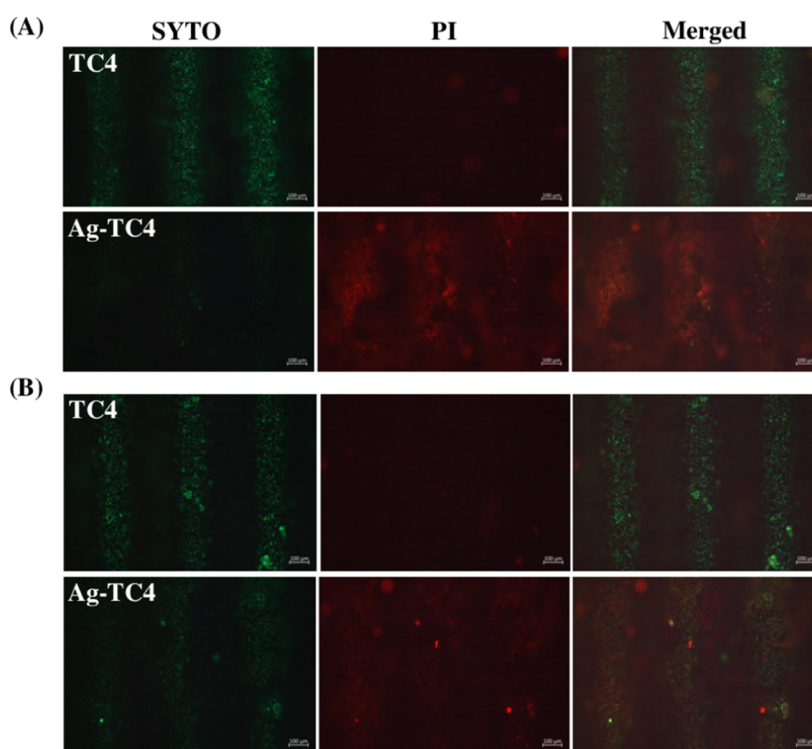
Figure 5. Fluorescence microscope images of Live/Dead staining: *S. aureus* (A) and *E. coli* (B) on the TC4 and Ag-TC4 surfaces. The viable cells appeared green, while the nonviable cells appeared red. Experiments were repeated three times, and each sample was observed in five random fields under the fluorescence microscope.
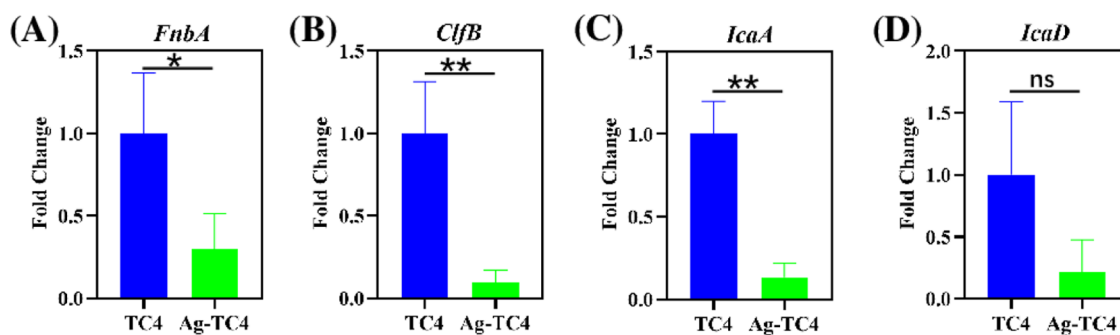

Figure 6. Expression of adhesion and biofilm-associated genes in *S. aureus* growing on the TC4 and Ag-TC4 surfaces: (A) *FnbA*. (B) *ClfB*. (C) *IcaA*. (D) *IcaD*. (Values are mean ± standard deviation, *represents $P < 0.05$, **represents $P < 0.01$, TC4 vs Ag-TC4, and every result was obtained from three independent experiments).

The live/dead staining technique was used to identify the biofilm formation on TC4 and Ag-TC4 samples. As shown in Figure 5, it can be seen that the surface of TC4 displays a large piece of green, indicating a large number of live bacteria and a thick and dense biofilm. In contrast, the surface of Ag-TC4 is mostly stained red or orange, indicating a large number of dead bacteria and a loose biofilm. These results prove that the presence of silver affects the formation and activity of bacterial biofilms, and that the introduction of Ag$^+$ on the surface of titanium alloys by EDM can give titanium implants some antibacterial and antibacterial biofilm effects.

A similar conclusion was reached by Nakajo[49] et al., who observed the formation of *Streptococcus mutants* and *Streptococcus* distant biofilms on the surface of titanium–silver alloys with different silver contents and concluded that the amount of biofilm formation on Ti–20% Ag and Ti–25% Ag alloys was significantly lower than that on pure titanium alloys, but the silver ions in the alloys were not released under physiological conditions due to the easy formation of a titanium oxide layer on the surface of the alloys, so the titanium–silver alloys did not have an antibacterial or bactericidal effect in this study.

In our current research, silver was deposited on the surface of the titanium microgrooved surface, and Ag$^+$ was produced from the metallic silver after hydrolysis and had a bactericidal and antibiofilm effect. Probably because Ag$^+$ on the surface were not wrapped or covered by the alloy, they can approach and penetrate the biofilm, and then disrupt the biofilm structure and interact with key components of the biofilm, such as polysaccharides, proteins, nucleic acids, and lipids, through electrostatic, hydrophobic, hydrogen bonding, and van der Waals interactions, which can impede the activity of the biofilm.[50]

2.6. qRT-PCR. We further investigated the bacteriostatic efficacy of Ag-TC4 at the genetic level. The polysaccharide intercellular adhesin (PIA), an important component of the extracellular polymer of staphylococcal biofilms, plays an important role in the formation of the *S. aureus* biofilm. The primary genes encoding PIA are *icaA*, *icaD*, *icaB*, and *icaC*, which are negatively regulated by the *icaR* gene.[51] The expression of the ica motif is influenced by environmental conditions, with the product of *icaA*, an *N*-acetylaminoglucosyltransferase, synthesizing PIA oligomers from UDP-*N*-acetylaminoglucan, and the product of *icaD* providing optimal efficiency for *icaA*. *FnbA* encodes a fibronectin-binding protein, a key link between cells and their extracellular matrix, which plays an important role in early bacterial adhesion. *ClfB*, an MSCRAMM (microbial surface components recognizing adhesive matrix molecules) family surface protein, has been described as a fibrinogen-binding aggregation factor and is a key determinant of *S. aureus* colonization.[51] The results of real-time fluorescence PCR on the expression of the above-mentioned genes related to *S. aureus* adhesion and biofilm production showed that Ag-TC4 inhibited the expression of *fnbA* and *ClfB*, genes related to adhesion proteins, and *icaA* and *icaD*, genes related to biofilm synthesis, which were consistent with the results of live/dead fluorescence staining, and it can be assumed that Ag-TC4's antibiofilm effect is due to the modulation of bacterial adhesion and biofilm-related genes by the released Ag$^+$. Thus, the technique of EDM silver deposition is of some application in improving the antibacterial properties of titanium endosomes (Figure 6).

The use of the flexible brush electrode in EDM allows the construction of strong and homogeneous silver coatings on complex microgrooved surfaces. Its comprehensive properties in terms of resistance to bacterial adhesion, growth, and biofilm formation are promising for biomedical implants, particularly in orthopedics, dentistry, cardiovascular stents, and medical devices, as well as promising applications in food and industrial manufacturing due to its good antimicrobial properties.

3. CONCLUSIONS

The use of the flexible brush electrode in EDM enables silver to be uniformly deposited on the surface of complex titanium alloy microgrooves. The silver-containing microgrooved surface has good wettability and continuously releases silver ions, which inhibit the adhesion of *S. aureus* and *E. coli* on the surface of the samples, and disrupt the morphology and growth of the bacteria, and affect the formation of the *S. aureus* biofilm. This research could lay the groundwork for the study of antimicrobial metal bound to microstructured surfaces and pave the way for future implant surface design.

4. MATERIALS AND METHODS

4.1. Sample Preparation and Characterization. In this study, Ti$_6$Al$_4$V titanium alloy was used as the base material. The chemical composition and material properties of Ti$_6$Al$_4$V titanium alloy are shown in Tables 1 and 2 respectively. Samples (10 × 10 × 1 mm) were cut using a WEDM system (MV1200S, Mitsubishi Electric, Japan) to produce a sine wave-microgrooved surface (named TC4 group), as shown in Figure 7A. Wire speed, tension, and working fluid flow were 10 m/min, 3 N, and 11 L/min, respectively. Deionized water was used as the working medium. The parameters associated with sinusoidal microgrooves are shown in Figure 7B,C. The EDM

Table 1. Chemical Composition of Ti$_6$Al$_4$V

element	content (%)	element	content (%)
Ti	88.1−91.1	Si	<0.03
Al	5.5−6.8	N	<0.05
V	3.5−4.5	C	<0.01
Fe	<0.3	H	0.0048
O	<0.2		

Table 2. Material Properties of Ti$_6$Al$_4$V

density (kg/m^3)	thermal conductivity W/(m·k)	specific heat capacity (J/kg·C)	melting point (°C)
4510	7.955	582	3200

technique was then used to deposit silver on the microgrooved surface as follows: a metal cold welding repair machine (Hz3k-100A, Qixiong, China) was used as the power source, a silver wire brush of 5 mm diameter prepared from 0.2 mm wire diameter was used as the tool electrode, and the microgrooved workpiece was connected to the negative electrode of the power source at a voltage of 45 V, a pulse width of 50 μs, and a frequency of 50 Hz. The silver brush was connected to the positive terminal of the power supply, and the titanium microgrooved workpiece was connected to the negative terminal of the power supply and fed with 15 L/min argon gas for 1 min (Figure 7D). The preparation process for silver-containing microgrooves (named Ag-TC4 group) is shown in Figure 7E.

A scanning electron microscope (TM3030, Hitachi, Japan) and an X-ray diffractometer (D8 ADVANCE, Bruker, Germany) were used to observe and analyze the morphology and phase composition of the microgrooved surfaces. An X-ray photoelectron spectrometer (EScalaba 25Xi, Thermo Fisher, UK) was used to analyze the elemental species and the chemical state of the materials on the surface of the samples. The vacuum in the chamber was better than $5.0 \times 10{-}10$ mBar, and the X-ray source (Al target) has a beam spot of 650 μm and a voltage and current of 15 kV and 15 mA, respectively. A contact angle tester (XG-CAM, XuanYiChuang-Xi, China) was used to measure the contact angle of the surface in terms of the wetting properties. All samples were cleaned before the experiment using an ultrasonic cleaner, autoclaved, and dried.

4.2. Ion Release. The samples were immersed in sterile tubes containing 5 mL of deionized water for 1, 2, 4, 7, 11, and 14 days. The liquid samples were collected and then diluted 10 times. The silver ion concentrations were determined by inductively coupled plasma atomic emission spectroscopy (ICAP RQ, Thermo Fisher, USA).

4.3. Bacterial Strain Culture. *S. aureus* (sphere-shaped, Gram-positive) and *E. coli* (rod-shaped, Gram-negative), which are common pathogens for medical implant infections, were involved in this study. Frozen *S. aureus* and *E. coli* strains were streaked on an agar plate and incubated at 37 °C for a minimum of 12 h. Bacterial colonies on the agar plate were picked and inoculated in the Luria−Bertani (LB) liquid medium (10 g tryptone, 5 g yeast extract, and 10 g sodium chloride in 1000 mL distilled water, pH adjusted to 7.1, autoclaved for 20 min). Bacterial growth is tracked by measuring the optical density (OD) at 600 nm. Using the bacteria at the exponential phase of growth ensures that the bacteria remain in the same situation for subsequent experiments. The initial bacterial colony-forming unit (cfu)
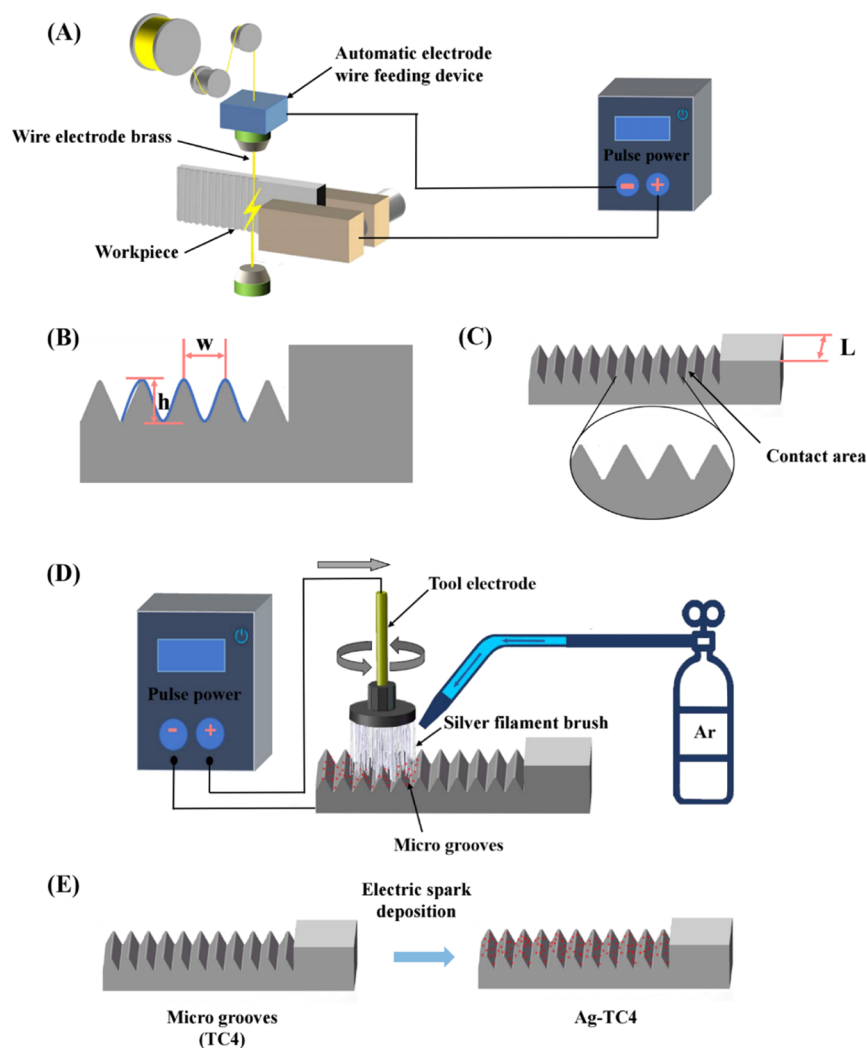
Figure 7. Samples processing methods and procedures: (A) schematic diagram for the preparation of microgrooves on the Ti$_6$Al$_4$V substrate using the WEDM machine. (B,C) Parameters associated with sinusoidal microgrooves. (D) Schematic diagram of EDM silver deposition on the surface of microgrooves. (E) Flow chart for the preparation of silver-containing microgrooves on the Ti$_6$Al$_4$V.
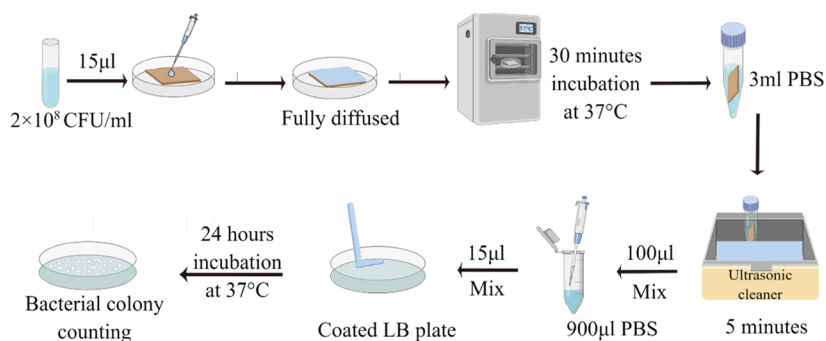

Figure 8. Schematic diagram of the process for testing the antimicrobial rate of samples by plate colony counting. (This diagram was made by Figdraw.)

density of the bacterial suspension can be calculated by multiplying the OD$_{600}$ value by 10^9 cfu/mL.

4.4. Bacterial Morphological Observation. A scanning electron microscope was used to observe the detailed morphologies of bacteria on the surface of the Ag-TC4 and TC4 samples. The samples were plated in a 24-well plate and subsequently immersed in an equivalent amount of bacterial suspension (500 μL) at a concentration of 5 × 10^7 cfu/mL.

After 1 h incubation at 37 °C, the samples were gently rinsed three times with phosphate-buffered solution (PBS) and then fixed for 4 h at 4 °C with 2.5 percent glutaraldehyde solution. The samples were dehydrated sequentially in a series of ethanol solutions with concentration gradients of 50, 60, 70, 80, 90, 95, and 100 v/v percent and then air dried until the anhydrous ethanol had evaporated before being observed with a scanning electron microscope.

4.5. Early Bacterial Adhesion. SYTO9 fluorescent dye (L7012 LIVE/DEAD BacLight Bacterial Viability Kit, Thermo Fisher, USA) was employed to stain the early adhered bacteria on the samples' surface. The samples were plated in a 24-well plate and subsequently immersed in an equivalent amount of bacterial suspension (500 μL) at a concentration of 5×10^7 cfu/mL. After 1 h incubation at 37 °C, the samples were gently rinsed three times with distilled water to remove any bacteria that had been poorly adherent and then incubated with SYTO9 at 6.68 μM for 20 min under sheltered conditions. Before the following characterization, the samples were gently rinsed with distilled water and dried in the air at room temperature. Live bacteria adhering to the surface of the samples appear green under an inverted fluorescence microscope (Axio Observer3, Zeiss, Germany).

4.6. Antibacterial Activity. The antimicrobial properties of the samples were evaluated using the method of bacterial counting (Figure 8). Briefly, the samples were placed in a 24-well plate, and 15 μL of *S. aureus* and *E. coli* at a concentration of 2×10^8 cfu/mL were added dropwise to the surface of the samples. After 30 min incubation at 37 °C, the samples were put into a sterilized centrifugal tube containing 3 mL of sterile PBS. Subsequently, the centrifugal tube was placed in an ultrasonic cleaner for 5 min to shake off the bacteria on the surface of the samples. Afterward, the dissociated bacterial suspension was collected and diluted 10 times with sterilized PBS. Following that, the 15 μL of diluted bacterial suspension were separately aspirated and uniformly coated on the LB agar plates with a sterile glass coating bar. Finally, the agar plates were inverted for 24 h at 37 °C in an incubator, and the colonies that survived were counted the next day. The antimicrobial rate of the samples was calculated using the formula

$$K = (\text{Nc} - \text{Ns})/\text{Nc} \times 100\%$$

where K is the antibacterial rate of the samples, and Nc and Ns represent the number of colonies on the LB agar plates of the TC4 and the Ag-TC4 samples, respectively.

4.7. Observation of Biofilm Staining. A LIVE/DEAD BacLight Bacterial Viability Kit (L7012) was employed to stain the biofilm on the TC4 and Ag-TC4 samples. Two nucleic acid dyes are included in the kit: propidium iodide (PI), which stains dead bacteria red, and SYTO9, which stains living bacteria green. The samples were placed in 24-well plates with 1 mL of *S. aureus* and *E. coli* at a concentration of 2.2×10^8 cfu/mL. After being incubated for 10 h at 37 °C, the surface of the samples was gently rinsed with distilled water three times to get rid of any floating bacteria and then incubated with a 1 μL:1 μL:3 mL mixture of SYTO9, PI, and distilled water for 20 min at room temperature in the dark. Before the following characterization, the samples were gently rinsed with distilled water and dried in the air at room temperature. Live bacteria in biofilms appear green, whereas damaged or dead bacteria appear red under an inverted fluorescence microscope.

4.8. qRT-PCR. Based on the results of the abovementioned studies on the antibacterial properties of Ag-TC4, we selected *S. aureus*, which has a strong biofilm-forming capacity for further studies on the antibacterial mechanism. The samples were plated in a 24-well plate and subsequently immersed in an equivalent amount of bacterial suspension (1 mL) at a concentration of 2.2×10^8 cfu/mL. After 10 h incubation at 37 °C, the samples were put into a sterilized centrifugal tube containing 3 mL of sterile PBS. Subsequently, the centrifugal

tube was placed in an ultrasonic cleaner for 5 min to shake off the bacteria on the surface of the samples, after which the bacterial suspension was centrifuged to collect the bacteria. The RNA was extracted by using the trizol reagent, and a NanoDrop2000 Ultra-micro spectrophotometer (Wilmington, DE, USA) and agarose gel electrophoresis were used to evaluate the purity and integrity of the total RNA. cDNA was synthesized by using FastKing gDNA Dispelling RT SuperMix (Tiangen, Beijing, China). Real-time polymerase chain reaction (RT-PCR) was used to quantify the genes associated with the biofilm of *S. aureus*, including *icaA*, *icaD*, *fnbA*, and *clfB* by using the CFX96 Touch fluorescence quantitative PCR detection system (Bio-Rad, Hercules, America). 16sRNA was the housekeeping gene. All the primer sequences used in this study are presented in Table 3. The mean cycle threshold (C_t) of all target genes was normalized to the housekeeping gene 16sRNA, and the $2^{-\Delta\Delta C_t}$ method was used to calculate mRNA fold changes.

Table 3. Primer Sequences Used for qRT-PCR Gene Expression Analysis

gene	primer sequences
16sRNA	F: 5′-CACGATGGAGGGGCCGGACTCATC-3′
	R: 5′-TAAAGACCTCTATGCCAACACAGT-3′
icaA	F: 5′-GTTGTCGACGTTGGCTACTG-3′
	R: 5′-TGCTTCCAAAGACCTCCCAA-3′
icaD	F: 5′-GGTCAAGCCCAGACAGAG-3′
	R: 5′-TGCTTCCAAAGACCTCCCAA-3′
clfB	F: 5′-GTCGTGAGATGTTGGGTT-3′
	R: 5′-CTTTATGGGATTTGCTTGA-3′
fnbA	F: 5′-ACCTCATGCAGGACAACGAG-3′
	R: 5′-TCGCC ATTAC GACTG AACCA-3′

4.9. Statistical Analysis. SPSS 25.0 (SPSS, Inc, an IBM Company, Chicago, IL, USA) was used to statistically analyze the data, which were expressed as mean ± standard deviation (SD); *t*-test analysis was used to evaluate the effect of EDM silver deposition on bacterial adherent growth and biofilm formation, and the difference was statistically significant at $P < 0.05$.

■ **AUTHOR INFORMATION**

Corresponding Author

Guie Xie — *Guangzhou Key Laboratory for Clinical Rapid Diagnosis and Early Warning of Infectious Diseases, KingMed School of Laboratory Medicine, Guangzhou Medical University, Guangzhou 510182, PR China;* ⊙ orcid.org/0000-0003-3772-1576; Email: guier2003@126.com

Authors

Kaihui Shi — *Guangzhou Key Laboratory for Clinical Rapid Diagnosis and Early Warning of Infectious Diseases, KingMed School of Laboratory Medicine, Guangzhou Medical University, Guangzhou 510182, PR China*

Hao Zhang — *State Key Laboratory of Precision Electronic Manufacturing Technology and Equipment, Guangdong University of Technology, Guangzhou 510006, PR China*

Yuyan Gu — *Guangzhou Key Laboratory for Clinical Rapid Diagnosis and Early Warning of Infectious Diseases, KingMed School of Laboratory Medicine, Guangzhou Medical University, Guangzhou 510182, PR China*

Zhijie Liang − *State Key Laboratory of Precision Electronic Manufacturing Technology and Equipment, Guangdong University of Technology, Guangzhou 510006, PR China*

Huanyu Zhou − *Guangzhou Key Laboratory for Clinical Rapid Diagnosis and Early Warning of Infectious Diseases, KingMed School of Laboratory Medicine, Guangzhou Medical University, Guangzhou 510182, PR China*

Haojie Liu − *Guangzhou Key Laboratory for Clinical Rapid Diagnosis and Early Warning of Infectious Diseases, KingMed School of Laboratory Medicine, Guangzhou Medical University, Guangzhou 510182, PR China*

Jiangwen Liu − *State Key Laboratory of Precision Electronic Manufacturing Technology and Equipment, Guangdong University of Technology, Guangzhou 510006, PR China*

Complete contact information is available at:
https://pubs.acs.org/10.1021/acsomega.2c06253

Author Contributions

§K.S. and H.Z. contributed equally to this work.

Notes

The authors declare no competing financial interest.

■ REFERENCES

(1) Iaquinta, M. R.; Mazzoni, E.; Manfrini, M.; D'Agostino, A.; Trevisiol, L.; Nocini, R.; Trombelli, L.; Barbanti-Brodano, G.; Martini, F.; Tognon, M. Innovative Biomaterials for Bone Regrowth. *Int. J. Mol. Sci.* **2019**, *20*, 618.

(2) Deng, Y.; Gao, X.; Shi, X.-L.; Lu, S.; Yang, W.; Duan, C.; Chen, Z.-G. Graphene Oxide and Adiponectin-Functionalized Sulfonated Poly(etheretherketone) with Effective Osteogenicity and Remotely Repeatable Photodisinfection. *Chem. Mater.* **2020**, *32*, 2180−2193.

(3) Wang, S.; Duan, C.; Yang, W.; Gao, X.; Shi, J.; Kang, J.; Deng, Y.; Shi, X. L.; Chen, Z. G. Two-dimensional nanocoating-enabled orthopedic implants for bimodal therapeutic applications. *Nanoscale* **2020**, *12*, 11936−11946.

(4) Deng, Y.; Shi, X.; Chen, Y.; Yang, W.; Ma, Y.; Shi, X.-L.; Song, P.; Dargusch, M. S.; Chen, Z.-G. Bacteria-Triggered pH-Responsive Osteopotentiating Coating on 3D-Printed Polyetheretherketone Scaffolds for Infective Bone Defect Repair. *Ind. Eng. Chem. Res.* **2020**, *59*, 12123−12135.

(5) Losic, D. Advancing of titanium medical implants by surface engineering: recent progress and challenges. *Expert Opin. Drug Delivery* **2021**, *18*, 1355−1378.

(6) Oliva, A.; Miele, M. C.; Al Ismail, D.; Di Timoteo, F.; De Angelis, M.; Rosa, L.; Cutone, A.; Venditti, M.; Mascellino, M. T.; Valenti, P.; et al. Challenges in the Microbiological Diagnosis of Implant-Associated Infections: A Summary of the Current Knowledge. *Front. Microbiol.* **2021**, *12*, 750460.

(7) Ascenzioni, F.; Cloeckaert, A.; Di Domenico, E. G.; Dunyach-Remy, C.; Guembe, M. Editorial: Microbial Biofilms in Chronic and Recurrent Infections. *Front. Microbiol.* **2021**, *12*, 803324.

(8) Shrestha, P.; Cooper, B. S.; Coast, J.; Oppong, R.; Do Thi Thuy, N.; Phodha, T.; Celhay, O.; Guerin, P. J.; Wertheim, H.; Lubell, Y. Enumerating the economic cost of antimicrobial resistance per antibiotic consumed to inform the evaluation of interventions affecting their use. *Antimicrob. Resist. Infect. Control* **2018**, *7*, 98.

(9) Arciola, C. R.; Campoccia, D.; Montanaro, L. Implant infections: adhesion, biofilm formation and immune evasion. *Nat. Rev. Microbiol.* **2018**, *16*, 397−409.

(10) Rabiee, N.; Ahmadi, S.; Akhavan, O.; Luque, R. Silver and Gold Nanoparticles for Antimicrobial Purposes against Multi-Drug Resistance Bacteria. *Materials* **2022**, *15*, 1799.

(11) Guo, C.; Cui, W.; Wang, X.; Lu, X.; Zhang, L.; Li, X.; Li, W.; Zhang, W.; Chen, J. Poly-l-lysine/Sodium Alginate Coating Loading Nanosilver for Improving the Antibacterial Effect and Inducing Mineralization of Dental Implants. *ACS Omega* **2020**, *5*, 10562−10571.

(12) Cai, Y.; Bing, W.; Chen, C.; Chen, Z. Gaseous Plastron on Natural and Biomimetic Surfaces for Resisting Marine Biofouling. *Molecules* **2021**, *26*, 2592.

(13) Shahali, H.; Hasan, J.; Mathews, A.; Wang, H.; Yan, C.; Tesfamichael, T.; Yarlagadda, P. Multi-biofunctional properties of three species of cicada wings and biomimetic fabrication of nanopatterned titanium pillars. *J. Mater. Chem. B* **2019**, *7*, 1300−1310.

(14) Ye, J.; Deng, J.; Chen, Y.; Yang, T.; Zhu, Y.; Wu, C.; Wu, T.; Jia, J.; Cheng, X.; Wang, X. Cicada and catkin inspired dual biomimetic antibacterial structure for the surface modification of implant material. *Biomater. Sci.* **2019**, *7*, 2826−2832.

(15) Riedel, J.; Vucko, M. J.; Blomberg, S. P.; Schwarzkopf, L. Skin hydrophobicity as an adaptation for self-cleaning in geckos. *Ecol. Evol.* **2020**, *10*, 4640−4651.

(16) Ge, X.; Ren, C.; Ding, Y.; Chen, G.; Lu, X.; Wang, K.; Ren, F.; Yang, M.; Wang, Z.; Li, J.; et al. Micro/nano-structured TiO2 surface with dual-functional antibacterial effects for biomedical applications. *Bioact. Mater.* **2019**, *4*, 346−357.

(17) Jannesari, M.; Akhavan, O.; Madaah Hosseini, H. R.; Bakhshi, B. Graphene/CuO2 Nanoshuttles with Controllable Release of Oxygen Nanobubbles Promoting Interruption of Bacterial Respiration. *ACS Appl. Mater. Interfaces* **2020**, *12*, 35813−35825.

(18) Akhavan, O.; Ghaderi, E. Escherichia coli bacteria reduce graphene oxide to bactericidal graphene in a self-limiting manner. *Carbon* **2012**, *50*, 1853−1860.

(19) Kim, M. G.; Park, C. H. The Topographical Optimization of 3D Microgroove Pattern Intervals for Ligamentous Cell Orientations: In Vitro. *Int. J. Mol. Sci.* **2020**, *21*, 9358.

(20) Jayaraman, M.; Meyer, U.; Bühner, M.; Joos, U.; Wiesmann, H.-P. Influence of titanium surfaces on attachment of osteoblast-like cells in vitro. *Biomaterials* **2004**, *25*, 625−631.

(21) Li, M.; Fu, X.; Gao, H.; Ji, Y.; Li, J.; Wang, Y. Regulation of an osteon-like concentric microgrooved surface on osteogenesis and osteoclastogenesis. *Biomaterials* **2019**, *216*, 119269.

(22) Xu, Z.; Chen, K.; Li, M.; Hu, C.; Yin, P. Sustained release of Ag + confined inside polyoxometalates for long-lasting bacterial resistance. *Chem. Commun.* **2020**, *56*, 5287−5290.

(23) Wang, Q.; Zhang, Y.; Li, Q.; Chen, L.; Liu, H.; Ding, M.; Dong, H.; Mou, Y. Therapeutic Applications of Antimicrobial Silver-Based Biomaterials in Dentistry. *Int. J. Nanomed.* **2022**, *17*, 443−462.

(24) Kang, M.-K.; Moon, S.-K.; Kwon, J.-S.; Kim, K.-M.; Kim, K.-N. Antibacterial effect of sand blasted, large-grit, acid-etched treated Ti-Ag alloys. *Mater. Res. Bull.* **2012**, *47*, 2952−2955.

(25) Akhavan, O. Lasting antibacterial activities of Ag-TiO2/Ag/a-TiO2 nanocomposite thin film photocatalysts under solar light irradiation. *J. Colloid Interface Sci.* **2009**, *336*, 117−124.

(26) Jin, J.; Zhang, L.; Shi, M.; Zhang, Y.; Wang, Q. Ti-GO-Ag nanocomposite: the effect of content level on the antimicrobial activity and cytotoxicity. *Int. J. Nanomed.* **2017**, *12*, 4209−4224.

(27) Akhavan, O.; Ghaderi, E. Capping antibacterial Ag nanorods aligned on Ti interlayer by mesoporous TiO2 layer. *Surf. Coat. Technol.* **2009**, *203*, 3123−3128.

(28) Park, S. W.; Lee, D.; Choi, Y. S.; Jeon, H. B.; Lee, C.-H.; Moon, J.-H.; Kwon, I. K. Mesoporous TiO2 implants for loading high dosage of antibacterial agent. *Appl. Surf. Sci.* **2014**, *303*, 140−146.

(29) Sumanth, P.; Vaishnav Reddy, M. V.; Shaik, I.; Maddu, J. R. Parameter Optimization of EDM Characteristics on Ti-6Al-4V Using Different Electrodes. *IOP Conf. Ser.: Mater. Sci. Eng.* **2021**, *1185*, 012022.

(30) Franci, G.; Falanga, A.; Galdiero, S.; Palomba, L.; Rai, M.; Morelli, G.; Galdiero, M. Silver nanoparticles as potential antibacterial agents. *Molecules* **2015**, *20*, 8856−8874.

(31) Agnihotri, S.; Mukherji, S.; Mukherji, S. Immobilized silver nanoparticles enhance contact killing and show highest efficacy: elucidation of the mechanism of bactericidal action of silver. *Nanoscale* **2013**, *5*, 7328−7340.

(32) Fu, S.; Zhang, Y.; Qin, G.; Zhang, E. Antibacterial effect of Ti Ag alloy motivated by Ag-containing phases. *Mater. Sci. Eng., C* **2021**, *128*, 112266.

(33) Souter, P.; Vaughan, J.; Butcher, K.; Dowle, A.; Cunningham, J.; Dodd, J.; Hall, M.; Wilson, D.; Horner, A.; Genever, P. Identification of mesenchymal stromal cell survival responses to antimicrobial silver ion concentrations released from orthopaedic implants. *Sci. Rep.* **2020**, *10*, 18950.

(34) Lu, M. M.; Ge, Y.; Qiu, J.; Shao, D.; Zhang, Y.; Bai, J.; Zheng, X.; Chang, Z. M.; Wang, Z.; Dong, W. F.; et al. Redox/pH dual-controlled release of chlorhexidine and silver ions from biodegradable mesoporous silica nanoparticles against oral biofilms. *Int. J. Nanomed.* **2018**, *13*, 7697−7709.

(35) Kumar, R.; Münstedt, H. Silver ion release from antimicrobial polyamide/silver composites. *Biomaterials* **2005**, *26*, 2081−2088.

(36) Xu, Z.; Zhang, C.; Wang, X.; Liu, D. Release Strategies of Silver Ions from Materials for Bacterial Killing. *ACS Appl. Bio Mater.* **2021**, *4*, 3985−3999.

(37) Mirzajani, F.; Ghassempour, A.; Aliahmadi, A.; Esmaeili, M. A. Antibacterial effect of silver nanoparticles on Staphylococcus aureus. *Res. Microbiol.* **2011**, *162*, 542−549.

(38) Minoura, K.; Yamada, M.; Mizoguchi, T.; Kaneko, T.; Nishiyama, K.; Ozminskyj, M.; Koshizuka, T.; Wada, I.; Suzutani, T. Antibacterial effects of the artificial surface of nanoimprinted moth-eye film. *PLoS One* **2017**, *12*, No. e0185366.

(39) Gusev, A.; Zakharova, O.; Vasyukova, I.; Muratov, D. S.; Rybkin, I.; Bratashov, D.; Lapanje, A.; Il'inikh, I.; Kolesnikov, E.; Kuznetsov, D. Effect of GO on bacterial cells: Role of the medium type and electrostatic interactions. *Mater. Sci. Eng., C* **2019**, *99*, 275−281.

(40) Yuan, Y.; Hays, M. P.; Hardwidge, P. R.; Kim, J. Surface characteristics influencing bacterial adhesion to polymeric substrates. *RSC Adv.* **2017**, *7*, 14254−14261.

(41) Zanna, S.; Mercier, D.; Gardin, E.; Allion-Maurer, A.; Marcus, P. EPS for bacterial anti-adhesive properties investigated on a model metal surface. *Colloids Surf., B* **2022**, *213*, 112413.

(42) Jiang, Y.; Yin, Y.-J.; Zha, X.-C.; Dou, X.-Q.; Feng, C.-L. Wettability regulated gram-negative bacterial adhesion on biomimetic hierarchical structures. *Chin. Chem. Lett.* **2017**, *28*, 813−817.

(43) Dou, X. Q.; Zhang, D.; Feng, C.; Jiang, L. Bioinspired Hierarchical Surface Structures with Tunable Wettability for Regulating Bacteria Adhesion. *ACS Nano* **2015**, *9*, 10664−10672.

(44) Chouirfa, H.; Bouloussa, H.; Migonney, V.; Falentin-Daudré, C. Review of titanium surface modification techniques and coatings for antibacterial applications. *Acta Biomater.* **2019**, *83*, 37−54.

(45) Siddiqi, K. S.; Husen, A.; Rao, R. A. K. A review on biosynthesis of silver nanoparticles and their biocidal properties. *J. Nanobiotechnol.* **2018**, *16*, 14.

(46) Ishida, T. Antibacterial mechanism of Ag+ ions for bacteriolyses of bacterial cell walls via peptidoglycan autolysins, and DNA damages. *MOJ Toxicol.* **2018**, *4*, 345.

(47) Del Pozo, J. L. Biofilm-related disease. *Expert Rev. Anti-Infect. Ther.* **2018**, *16*, 51−65.

(48) Yin, W.; Wang, Y.; Liu, L.; He, J. Biofilms: The Microbial "Protective Clothing" in Extreme Environments. *Int. J. Mol. Sci.* **2019**, *20*, 3423.

(49) Nakajo, K.; Takahashi, M.; Kikuchi, M.; Takada, Y.; Okuno, O.; Sasaki, K.; Takahashi, N. Inhibitory effect of Ti-Ag alloy on artificial biofilm formation. *Dent. Mater. J.* **2014**, *33*, 389−393.

(50) Joshi, A. S.; Singh, P.; Mijakovic, I. Interactions of Gold and Silver Nanoparticles with Bacterial Biofilms: Molecular Interactions behind Inhibition and Resistance. *Int. J. Mol. Sci.* **2020**, *21*, 7658.

(51) Nguyen, H. T. T.; Nguyen, T. H.; Otto, M. The staphylococcal exopolysaccharide PIA - Biosynthesis and role in biofilm formation, colonization, and infection. *Comput. Struct. Biotechnol. J.* **2020**, *18*, 3324−3334.